PASJ: Publ. Astron. Soc. Japan **51**, 837–850 (1999)

Search for Molecular Clouds toward Intermediate-to-High Latitude IRAS Sources in the Southern Sky

Yoshinori YONEKURA
Department of Earth and Life Sciences, Osaka Prefecture University, Sakai, Osaka 599-8531
E-mail (YY): yonekura@el.cias.osakafu-u.ac.jp
and
Takahiro HAYAKAWA, Norikazu MIZUNO, Yoshihiro MINE, Akira MIZUNO,
Hideo OGAWA,* and Yasuo FUKUI
Department of Astrophysics, Nagoya University, Chikusa-ku, Nagoya 464-8602

(Received 1999 April 19; accepted 1999 July 11)

Abstract

We have conducted a search for molecular clouds toward southern IRAS point sources at intermediate-to-high galactic latitude ($|b| \geq 10°$) in ^{12}CO ($J = 1$–0) emission with the NANTEN telescope. The main purpose of the survey was to find a new sample of star-forming clouds unknown to date. Of the 29 targets, we detected CO emission toward 5 IRAS sources, i.e., 04591−0856, 05044−0325, 05050−0614, 06345−3023, and 13543−3941. Among 5 detections, the molecular cloud associated with 06345−3023 (G 239.2−16.3) was detected for the first time. If we assume the distance as being 1.5 kpc, this source is ~ 430 pc away from the galactic plane. Three sources 04591−0856 (G 208.3−28.4), 05044−0325 (G 203.5−24.7), and 05050−0614 (G 206.4−25.9) are located west to the Orion molecular clouds, and 13543−3941 (G 316.4+21.2) is located in the cometary globule CG 12. Four of the 5 clouds show a cometary shape with a "head-tail" distribution, and three of them have the IRAS source located at the edge opposite to the tail. We find that all of the CO clouds are associated with the optical nebulosities, which are likely to be reflection nebulae. A comparison of the present CO clouds with those in Ophiuchus, Taurus, Chamaeleon, and L 1333 indicates that star-forming clouds tend to have a high column density, as well as a smaller ratio of the virial mass to the LTE mass.

Key words: ISM: clouds — ISM: molecules — radio lines: ISM — stars: formation

1. Introduction

Star formation occurs in interstellar molecular clouds. Several extensive surveys using the emission lines of CO and its isotopes were undertaken toward the galactic plane to reveal the distribution of the molecular gas (see Combes 1991 for a review). However, most of them are of small-latitude coverages, or of low angular resolutions, or of both. Two surveys with a moderate-to-high resolution and large latitude coverage are now underway. One is the Nagoya survey (Fukui, Yonekura 1997; Dobashi et al. 1994; Dobashi et al. 1996; Yonekura et al. 1997; Kawamura et al. 1998) with a moderate effective resolution of $8'$ in ^{13}CO ($J = 1$–0), which covers up to $|b| \sim 10°$–$20°$. The other is the FCRAO survey (Heyer et al. 1998) with a resolution of $1'$ in ^{12}CO ($J = 1$–0). These two surveys are providing a fairly extensive sample for star-forming molecular clouds. At high galactic latitude (usually taken to mean $|b| \gtrsim 25$–$30°$), after the initial survey of high-latitude molecular clouds by Blitz, Magnani, and Mundy (1984), more than 100 molecular clouds have been identified until now (Magnani et al. 1985; Keto, Myers 1986; see the up-to-date compilation by Magnani et al. 1996) and a systematic survey for high-latitude molecular clouds is in progress by a few groups (Hartmann et al. 1998; Onishi et al. 1999 in preparation). Most of the CO clouds at high latitude, however, show no sign of star formation, except for a few cases (e.g., Magnani et al. 1995).

The IRAS point source catalog is a useful database to search for young stellar objects embedded in molecular clouds. Sources selected by the infrared colors constitute a good sample of young stellar objects (e.g., Emerson 1987). In order to obtain a sample of star-forming clouds at intermediate-to-high galactic latitude, most of which may have never been studied in molecular emission, we have conducted a search for molecular clouds toward the IRAS point sources. We present the results of this search toward 29 isolated IRAS point sources with cold infrared spectra. In section 2, we describe the selection criteria for

* Present address: Department of Earth and Life Sciences, Osaka Prefecture University, Sakai, Osaka 599-8531.

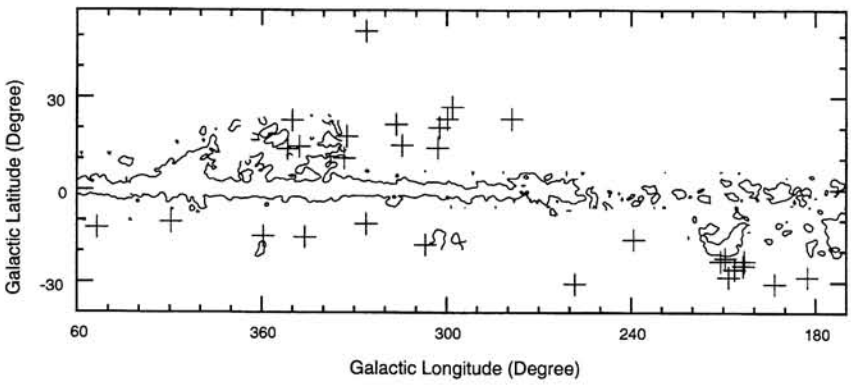

Fig. 1. Distribution of the target in galactic coordinates. The contours are taken from Dame et al. (1987).

our target list as well as the observations. In section 3, the results of the search are presented, and physical parameters of the detected molecular clouds are derived from the data. In section 4, we discuss the properties of these molecular clouds. The main results are summarized in section 5.

2. Observational Procedure

2.1. Source Selection

In order to select candidates for recently formed stars among the IRAS point sources, we investigated the infrared spectra of IRAS sources. IRAS sources embedded in molecular clouds tend to occupy fairly confined regions in an infrared color–color diagram (e.g., Emerson 1987). A large-scale survey for molecular clouds recently undertaken at Nagoya University reveals that IRAS sources inside ^{13}CO clouds tend to have cold infrared spectra (Yonekura et al. 1997).

We searched for sources having cold infrared spectra defined at 12, 25, and 60 μm, i.e., $\log(F_{12}/F_{25}) \leq -0.3$ and $\log(F_{25}/F_{60}) \leq 0.0$, where F_λ is the flux density detected in IRAS λ-μm band, with the data quality being better than or equal to 2 in 25 and 60 μm band. Since some galaxies and planetary nebulae have similar colors as young stellar objects (e.g., Pottasch 1992), we excluded sources identified as extragalactic sources or planetary nebulae in the literature by using a database, such as NASA Extragalactic Database (NED) at IPAC.

The main purpose of this work was to discover nearby star-forming clouds unknown to date. We thus restricted targets located at intermediate-to-high latitude, i.e., $|b| \geq 10°$. Sources located within or near to the well-known star-forming regions were also excluded. Finally, we selected sources with $\delta \leq +30°$, which are accessible from the NANTEN telescope at Las Campanas Observatory, Chile.

The selection criteria described above produced a target list of 29 IRAS point sources. The distribution of targets is shown in figure 1.

2.2. Observations

Observations were made with the NANTEN millimeter-wave telescope of Nagoya University. The NANTEN telescope was installed in 1996 March at Las Campanas Observatory, Chile, under collaboration between Nagoya University and Carnegie Institution of Washington. The main-dish diameter of the NANTEN telescope is 4-meter, providing a half-power beam width of 2.′7 at 110 GHz. The 4 K cooled SIS mixer receiver provided a typical system temperature of 140 K (SSB) at 110 GHz and 200 K (SSB) at 115 GHz, including the atmosphere toward the zenith (Ogawa et al. 1990). The NANTEN telescope was equipped with two acousto-optical spectrometers having 2048 channels. One is the high-resolution AOS (AOS-H) with a total bandwidth and a frequency resolution of 40 MHz and 40 kHz, respectively; the other is the wide-band AOS (AOS-W) with a total bandwidth and a frequency resolution of 250 MHz and 250 kHz, respectively.

First, we made 5×5 mapping observations toward 29 IRAS sources at a $2'$ grid spacing in the $J = 1$–0 line of ^{12}CO. Observations were made from 1997 September to 1997 October. All of the data were obtained using a "multi-on-off" position-switching technique, i.e., more than two on positions were observed with a common off-position measurement. We used the AOS-W spectrometer centered at $V_{\rm LSR} = 0$ km s^{-1}. The velocity covered by the observations was $|V_{\rm LSR}| \lesssim 300$ km s^{-1}, which was large enough to detect all of the emission from galactic sources. Each point was observed for a total integration time of ~ 30 s, and the typical rms noise of the data was

$\Delta T_{\rm rms} \sim 0.2$ K at a velocity resolution of 0.65 km s^{-1}.

Second, we mapped the IRAS sources detected in the first step in ^{12}CO, ^{13}CO, and C^{18}O. All of the observations in this second step were made by using the AOS-H spectrometer. The ^{12}CO data were obtained from 1997 September to 1997 October. The central portion of the cloud was observed with a grid spacing of 2′ by using a "multi-on-off" position-switching technique, and the rest with 4′ grid using a frequency-switching technique with a switching interval of 13 MHz. The total integration time and the typical rms noise of the data at a velocity resolution of 0.1 km s^{-1} were $\sim$ 20 s and $\Delta T_{\rm rms} \sim 0.45$ K for the frequency-switching observations and $\sim$ 40 s and $\sim$ 0.3 K for the position-switching observations. In ^{13}CO, observations were made in 1998 February and in 1999 March with 2′ grid by using a frequency-switching technique with a switching interval of 13 MHz. The total integration time per point was $\sim$ 20 s and the typical rms noise of the data was $\Delta T_{\rm rms} \sim 0.3$ K at a velocity resolution of 0.1 km s^{-1}. C^{18}O observations were made in 1998 March, July, August, and in 1999 March. The data were obtained with a grid spacing of 2′ by using a frequency-switching technique with a switching interval of 13 MHz. The total integration time per point was $\sim$ 2 min. The typical rms noise of the data was $\Delta T_{\rm rms} \sim 0.1$ K at a velocity resolution of 0.1 km s^{-1}.

For the calibration of the spectral line intensity, a room-temperature chopper wheel was employed. The absolute intensity calibration was made by observing more than one of the following sources every 2 hours: Ori KL [$\alpha(1950) = 5^{\rm h}32^{\rm m}47\overset{\rm s}{.}0$, $\delta(1950) = -5°24'21''$], ρ Oph East [$\alpha(1950) = 16^{\rm h}29^{\rm m}20\overset{\rm s}{.}9$, $\delta(1950) = -24°22'13''$], and TMC 1 [$\alpha(1950) = 4^{\rm h}38^{\rm m}42\overset{\rm s}{.}0$, $\delta(1950) = 25°35'45''$]. The peak radiation temperatures, $T_{\rm R}^*$, of Ori KL and ρ Oph East are taken to be 65 K and 15 K for ^{12}CO, and 10 K and 10 K for ^{13}CO, respectively, and we assumed $T_{\rm R}^*$(C^{18}O, ρ Oph East) = 4.4 K and $T_{\rm R}^*$(C^{18}O, TMC 1) = 2 K. The pointing accuracy was measured to be better than 20″, as checked by optical observations of stars with a CCD camera attached to the telescope as well as by radio observations of Jupiter, Venus, and the edge of the Sun.

3. Results

3.1. Results of the Search for Molecular Clouds

Among 29 targets, ^{12}CO emission was detected toward 5 IRAS sources, i.e., 04591−0856, 05044−0325, 05050−0614, 06345−3023, and 13543−3941. Three of them are at $20° \leq |b| < 30°$, and the other two are at $10° \leq |b| < 20°$. No CO emission was detected toward 3 sources at $|b| \geq 30°$. One of the 5 detections, the molecular cloud associated with IRAS 06345−3023 (G 239.2−16.3; we named molecular clouds according to the position of the IRAS sources in the galactic coordinates) was detected for the first time. Three sources 04591−0856 (G 208.3−28.4), 05044−0325 (G 203.5−24.7), and 05050−0614 (G 206.4−25.9) were located west to the Orion complex and IRAS 13543−3941 (G 316.4+21.2) is associated with the cometary globule CG 12. The results of the observations are summarized in table 1 as well as the infrared properties and the optical counterparts. Comments on the detections are presented in subsection 3.3.

Here, we estimate the detection limit of the ^{12}CO observations. The noise level of the integrated intensity is estimated by measuring the dispersion of the CO intensity integrated over a velocity range of 5 km s^{-1}, about twice the typical value of the line width for high-latitude clouds (Magnani et al. 1996). The result indicates that the 3σ noise level in the integrated intensity is $\sim$ 1.5 K km s^{-1}. We assume the distance of targets as being 100 pc, and that the CO-to-H_2 conversion factor as being $N(H_2)/W(CO) = 2 \times 10^{20}$ cm^{-2} (K km s^{-1})$^{-1}$, where $N(H_2)$ and $W(CO)$ are the column density of H_2 and the CO integrated intensity, respectively (Magnani, Onello 1995). By taking the size of the cloud to be the same as the observing grid, 2′, the detection limit of molecular clouds is estimated to be $\sim 0.02\,M_\odot$.

3.2. Molecular Gas Distribution around the IRAS Sources

In order to investigate the physical properties of the molecular clouds, we made ^{12}CO, ^{13}CO, and C^{18}O mapping observations toward the detected 5 IRAS sources. The spatial distribution of the ^{12}CO, ^{13}CO, and C^{18}O integrated intensity is shown in figures 2–6. Optical images taken from the Digitized Sky Survey are also presented. Distributions of the molecular clouds are fairly similar to those of the nebulosities. Four of the 5 clouds have a cometary shape with "head-tail" distribution, and three of them, G 203.5−24.7, G 206.4−25.9, and G 316.4+21.2, have the IRAS source located at the edge of the cloud opposite to the tail. In order to see the velocity structure, we present position–velocity maps along the major axis in figure 7. Two clouds, G 208.3−28.4 and G 206.4−25.9, show a small velocity gradient around ~ 0.2 km s^{-1} pc^{-1}.

Table 2 lists the observed properties of the molecular clouds. The peak temperatures, $T_{\rm R}^*$, the LSR velocities, $V_{\rm LSR}$, and the line widths at half-maximum, ΔV, at the peak positions of the ^{12}CO, ^{13}CO, and C^{18}O integrated intensity maps were estimated using a single Gaussian fitting. The offsets of the peak positions of the C^{18}O integrated intensity map from the IRAS point sources are also presented in the table.

The physical properties of the molecular clouds are estimated in the following manner: For the ^{12}CO observa-

Table 1. Properties of the observed IRAS point sources.

IRAS name	Position l (°)	b (°)	α (1950) (^{h} ^{m} ^{s})	δ (1950) (° ′ ″)	Flux density F_{12} (Jy)	F_{25} (Jy)	F_{60} (Jy)	F_{100} (Jy)	Correlation coefficient	L^* ($L_\odot$)	Optical counterpart
Detections											
04591−0856	208.322	−28.433	4 59 6.6	−8 56 32	0.39	1.35	2.55	17.76	CAAG	0.28	y†
05044−0325	203.531	−24.704	5 4 25.8	−3 25 8	13.10	38.57	232.4	381.8	FBBB	8.84	?†
05050−0614	206.362	−25.897	5 5 2.6	−6 14 20	0.33:	0.78	3.22:	<32.31	FCCA	<0.42	?†
06345−3023	239.226	−16.316	6 34 34.7	−30 23 10	0.31	1.04	3.49	10.87	CAAA	0.20	y†
13543−3941	316.435	21.203	13 54 23.8	−39 41 21	<0.25	0.81	8.38:	<201.9	-BBG	<2.28	n†
Nondetections											
04108+1005	182.692	−28.409	4 10 52.5	10 5 10	1.15	6.43	26.32	37.21	BBDD	0.96	y†
04259+0116	193.418	−30.569	4 25 56.2	1 16 10	0.35	1.06	2.61	3.49	CBDC	0.12	y
05090−0226	203.202	−23.219	5 9 3.8	−2 26 25	0.25	1.20	1.79	<1.22	DAAF	<0.08	n
05222−0844	210.932	−23.224	5 22 13.4	−8 44 39	0.67	2.05	3.05	3.55	BAAA	0.17	y
05231−0701	209.376	−22.263	5 23 7.0	−7 1 55	<0.25	0.70	0.80	<1.08	FBB-	<0.05	y
05460−5104	258.363	−30.613	5 46 5.4	−51 4 55	3.46	9.05	19.90	11.28	AAAA	0.80	y
10594−3426	278.678	22.955	10 59 29.9	−34 26 7	0.70	2.44	3.92	5.04	BAAA	0.20	y
12272−3532	298.047	26.841	12 27 16.1	−35 33 0	<0.25	0.60	0.78	<1.00	-BC-	<0.05	y
12333−3935	299.722	22.906	12 33 19.3	−39 35 40	<0.43	3.38:	7.36:	3.81	FAAA	<0.24	y
12456−4226	302.345	20.160	12 45 40.0	−42 26 10	<0.25	1.02	2.70	1.43:	HAAB	<0.09	y
12481−4903	302.852	13.541	12 48 7.2	−49 3 32	<0.25	1.18	1.46	<1.95	-AAG	<0.08	y
13458−0823	326.049	51.657	13 45 50.9	−8 23 14	<0.25	1.03	16.78:	57.42	-CFB	<0.87	n
13545−4645	314.504	14.370	13 54 31.8	−46 45 54	<0.25	0.71	1.95	<1.45	-BAI	<0.07	y
14163−7952	306.937	−17.954	14 16 18.1	−79 52 54	0.31	0.70	6.05	10.04:	ADIE	0.22	y
15126−3658	332.394	17.323	15 12 37.5	−36 58 15	1.59	6.71	25.61	25.69	AAAA	0.87	y‡
15373−4220	333.230	10.197	15 37 22.5	−42 20 14	4.11	18.14	19.30	13.94	AAAA	1.07	y
15572−2234	350.010	22.446	15 57 15.6	−22 34 10	<0.43	1.45	4.05	<10.21	GGGF	<0.22	n
16178−3006	347.763	13.871	16 17 50.8	−30 6 37	<0.25	0.70	0.92	<3.40	IBBG	<0.08	y
16316−2749	351.595	13.185	16 31 39.3	−27 49 20	<0.25	0.69:	0.99	<12.91	-DCI	<0.18	n
16399−6247	326.201	−11.111	16 39 58.8	−62 47 54	<0.25	1.28	1.94	<2.18	FAAD	<0.09	y
18183−4827	345.983	−15.428	18 18 22.4	−48 27 42	<0.25	0.52	0.67	<2.60	GBCF	<0.06	y
18454−3620	359.559	−15.159	18 45 24.6	−36 20 23	<0.27	0.57	1.46	1.80	IBAC	<0.07	n
19205−0746	29.644	−10.550	19 20 34.5	−7 46 46	<0.25	0.55	2.88	3.05	-BAB	<0.10	y
20124+1154	53.600	−12.386	20 12 28.9	11 54 37	<0.25	0.86	0.97	<1.29	DABG	<0.06	n

*The luminosities are calculated following Myers et al. (1987). The distances are assumed to be 100 pc.
†Associated with nebulosities.
‡An object like a galaxy exists near the IRAS position.

tions, we calculate $N(\mathrm{H_2})$ from

$$N(\mathrm{H_2})/W(^{12}\mathrm{CO}) = 2 \times 10^{20}\,\mathrm{cm^{-2}(K\,km\,s^{-1})^{-1}}, \quad (1)$$

where $W(^{12}\mathrm{CO})$ is the integrated intensity (Magnani, Onello 1995). For ^{13}CO and C^{18}O, we assume the local thermodynamical equilibrium. The excitation temperature, T_{ex}, was estimated from $T_{\mathrm{R}}^*(^{12}\mathrm{CO})$ at the peak position of the ^{12}CO integrated intensity map by using

$$T_{\mathrm{ex}} = \frac{5.53}{\ln\{1 + 5.53/[T_{\mathrm{R}}^*(^{12}\mathrm{CO})(\mathrm{K}) + 0.819]\}}(\mathrm{K}). \quad (2)$$

We assumed that T_{ex} is uniform within the cloud. In order to derive the ^{13}CO and C^{18}O column densities, we divide a spectrum into 0.1 km s^{-1} bin, calculate the column density within each bin, and sum them up within a velocity range in which the intensity is larger than 3σ. The optical depth of ^{13}CO and C^{18}O line in each bin, $\tau_{13}(V)$ and $\tau_{18}(V)$, respectively, is calculated by using the following equations:

$$\tau_{13}(V) = -\ln\left(1 - \frac{T_{13}(V)}{5.29 \cdot \{J_{13}[T_{\mathrm{ex}}(\mathrm{K})] - 0.164\}}\right) \quad (3)$$

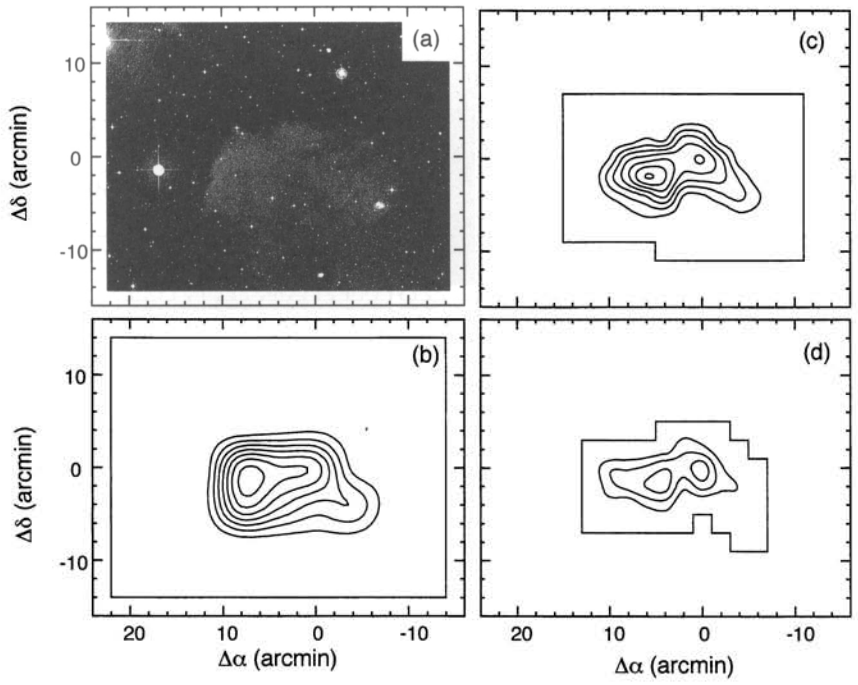

Fig. 2. (a) Optical image around IRAS 04591−0856 (G 208.3−28.4) taken from the Digitized Sky Survey. (b) Integrated intensity map of ^{12}CO. The contours are every 2.0 K km s^{-1} (5σ), starting from 2.0 K km s^{-1} (5σ). The solid line shows the observed area. (c) Integrated intensity map of ^{13}CO. The contours are every 0.6 K km s^{-1} (5σ), starting from 0.6 K km s^{-1} (5σ). (d) Integrated intensity map of C^{18}O. The contours are every 0.12 K km s^{-1} (3σ), starting from 0.12 K km s^{-1} (3σ).

Table 2. Observed properties of the molecular clouds.

Cloud name	Associated IRAS source	^{12}CO (J = 1–0) T_R^* (K)	V_{LSR} (km s^{-1})	ΔV (km s^{-1})	^{13}CO (J = 1–0) T_R^* (K)	V_{LSR} (km s^{-1})	ΔV (km s^{-1})	C^{18}O (J = 1–0) T_R^* (K)	V_{LSR} (km s^{-1})	ΔV (km s^{-1})	Offset†
G 208.3−28.4-East	04591−0856	13.1	4.9	1.1	4.5	4.9	0.8	1.1	5.0	0.4	(4′, −2′)
G 208.3−28.4-Center	04591−0856	8.5	4.7	1.1	4.0	4.6	0.7	0.9	4.7	0.4	(0, 0)
G 203.5−24.7	05044−0325	17.8	7.9	3.0	7.9	7.6	1.9	1.7	7.6	1.6	(−4, 0)
G 206.4−25.9	05050−0614	13.0	−2.0	1.9	6.0	−2.1	1.1	1.9	−2.2	0.6	(−2, 0)
G 239.2−16.3	06345−3023	5.4	17.2	1.6	2.2	17.4	0.9	0.5	17.5	0.5	(−2, 0)
G 316.4+21.2	13543−3941	16.8	−6.4	1.9	6.7	−6.2	1.6	1.6	−5.9	1.4	(2, 0)

†Offset of the peak positions of the C^{18}O (J = 1–0) integrated intensity map from the IRAS point sources in (α, δ).

and

$$\tau_{18}(V) = -\ln\left(1 - \frac{T_{18}(V)}{5.27 \cdot \{J_{18}[T_{ex}(\mathrm{K})] - 0.166\}}\right), \quad (4)$$

where $T_{13}(V)$ and $T_{18}(V)$ are the average temperatures of the ^{13}CO and C^{18}O spectrum in each bin in units of Kelvin, respectively, $J_{13}[T(\mathrm{K})] = 1/\{\exp[5.29/T(\mathrm{K})] - 1\}$, and $J_{18}[T(\mathrm{K})] = 1/\{\exp[5.27/T(\mathrm{K})] - 1\}$. The ^{13}CO and C^{18}O column densities, N_{13} and N_{18}, respectively, are estimated from the following equations:

$$N_{13} = 2.42 \times 10^{14} \times \sum_V \left\{\frac{0.1(\mathrm{km\ s^{-1}})\ \tau_{13}(V)\ T_{ex}(\mathrm{K})}{1 - \exp[-5.29/T_{ex}(\mathrm{K})]}\right\} (\mathrm{cm^{-2}}) \quad (5)$$

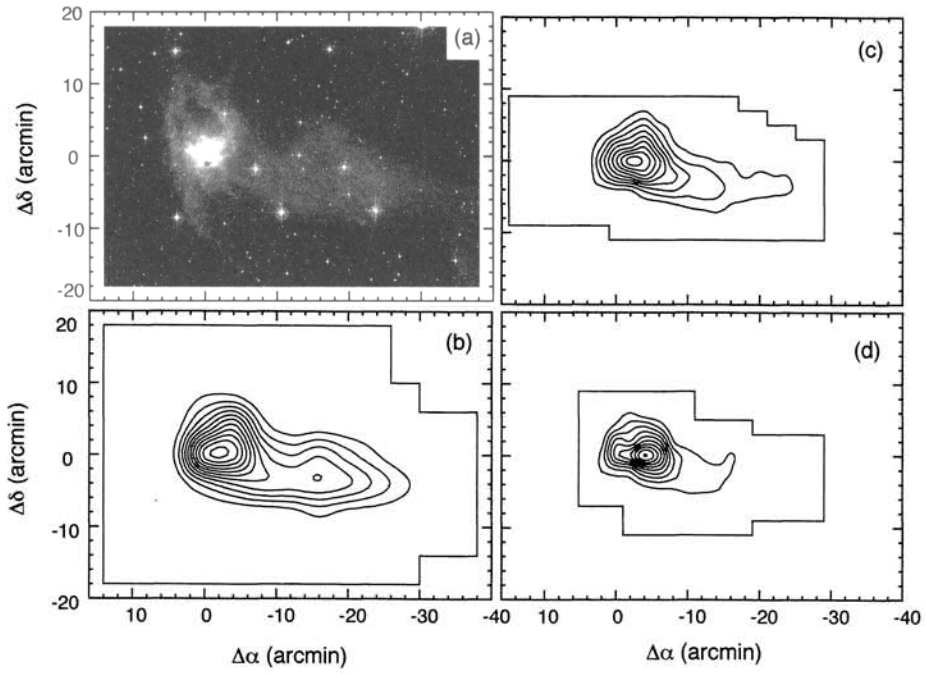

Fig. 3. Same as figure 2, but for IRAS 05044−0325 (G 203.5−24.7). The contour levels are every 4.83 K km s^{-1} (10σ), starting from 4.83 K km s^{-1} (10σ) in ^{12}CO, every 1.8 K km s^{-1} (15σ), starting from 1.8 K km s^{-1} (15σ) in ^{13}CO, and every 0.28 K km s^{-1} (5σ), starting from 0.28 K km s^{-1} (5σ) in C^{18}O.

and

$$N_{18} = 2.42 \times 10^{14} \times \sum_V \left\{ \frac{0.1(\mathrm{km\,s^{-1}})\,\tau_{18}(V) T_{\mathrm{ex}}(\mathrm{K})}{1 - \exp[-5.27/T_{\mathrm{ex}}(\mathrm{K})]} \right\} (\mathrm{cm^{-2}}). \quad (6)$$

The ratio $N(\mathrm{H_2})/N(^{13}\mathrm{CO})$ is assumed to be 5×10^5 (Dickman 1978), and we assume $N(\mathrm{H_2}) = [N(\mathrm{C^{18}O})/(1.7 \times 10^{14}) + 1.3] \times 10^{21}$ (Frerking et al. 1982).

The mass of each cloud is estimated by using

$$M = 2.8\, m_{\mathrm{H}} \sum [\, D^2 \Omega N(\mathrm{H_2})\,], \quad (7)$$

where D is the distance of the cloud, Ω is the solid angle subtended by the effective beam size ($4' \times 4'$ for ^{12}CO observations, and $2' \times 2'$ for ^{13}CO and C^{18}O observations), m_{H} is the proton mass, and the factor of 2.8 is the mean molecular weight per $\mathrm{H_2}$ molecule. The summation is performed over the observed points within the cloud. In order to derive the total mass of the cloud, we define a cloud at a 3σ contour in the integrated intensity map.

For ^{13}CO and C^{18}O observations, we also define a "core" at a 50% level of the integrated intensity at the peak position. The mass of the core is derived by using equation (7). The radius of the core, R, is calculated using

$$R = \sqrt{\frac{S}{\pi}}, \quad (8)$$

where S is the area inside the core. We also calculated the virial mass, M_{vir},

$$\left(\frac{M_{\mathrm{vir}}}{M_\odot}\right) = 209 \left(\frac{R}{\mathrm{pc}}\right) \left(\frac{\Delta V_{\mathrm{comp}}}{\mathrm{km\,s^{-1}}}\right)^2, \quad (9)$$

with ΔV_{comp} defined as the FWHM line width of the composite profile derived by using a single Gaussian fitting, where the composite profile is obtained by averaging all the spectra within the core. The average $\mathrm{H_2}$ density, $n(\mathrm{H_2})$, in the core was derived by dividing M by the volume of the core on the assumption that the core is spherical with radius R.

Table 3 summarizes the mass of each cloud derived for various molecular emissions. The physical properties of the ^{13}CO cores and the C^{18}O cores are listed in table 4 and table 5, respectively.

3.3. *Comments on Individual Objects*

In this subsection, detailed descriptions of the detections are presented.

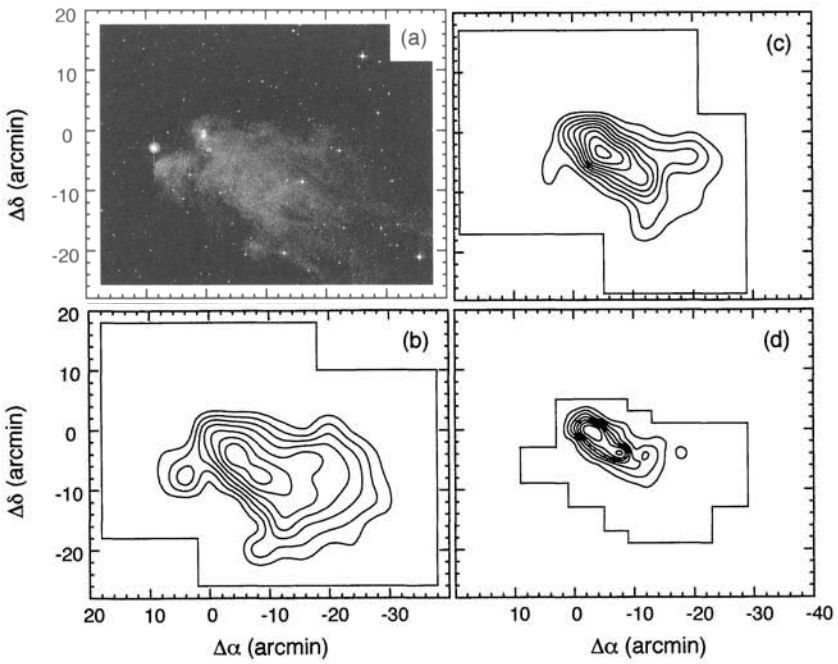

Fig. 4. Same as figure 2, but for IRAS 05050−0614 (G 206.4−25.9). The contour levels are every 2.83 K km s^{-1} (10σ), starting from 2.83 K km s^{-1} (10σ) in ^{12}CO, every 0.75 K km s^{-1} (7σ), starting from 0.75 K km s^{-1} (7σ) in ^{13}CO, and every 0.16 K km s^{-1} (3σ), starting from 0.16 K km s^{-1} (3σ) in C^{18}O.

Table 3. Masses of the molecular clouds.

Cloud name	^{12}CO mass ($M_\odot$)	^{13}CO mass ($M_\odot$)	C^{18}O mass ($M_\odot$)
G 208.3−28.4	95	54	85
G 203.5−24.7	530	350	440
G 206.4−25.9	540	230	250
G 239.2−16.3	1400	160	43
G 316.4+21.2	940	470	580

3.3.1. 04591−0856 (G 208.3−28.4)

This source is located $\sim 10°$ west to the Orion A molecular cloud. A reflection nebula, DG 49 (= LBN 968), is associated with the source. The nebulosity is located at the tail of a huge structure of roughly cometary shape, Cometary Complex-A (Ogura, Sugitani 1998). This source is thought to be influenced by the Ori OB1 association (Bally et al. 1991; Ogura, Sugitani 1998), and the distance is thus assumed to be the same as that of the Orion molecular clouds, 460 pc. CO emission was detected only at one position with 20′ resolution, which made the source catalogued as a high-latitude cloud, MBM 21 (Magnani et al. 1985). Further mapping observations in ^{12}CO and NH_3 were made (Stacy et al. 1989).

Our observation revealed that there are two intensity peaks in ^{13}CO and C^{18}O. One is at $(\Delta\alpha, \Delta\delta) = (4', -2')$ from the IRAS source and the other is at the IRAS position (figure 2). The emission from the eastern component is slightly stronger than the central one. In ^{12}CO, the cloud has a cometary shape with the head pointing toward east, the direction to the Ori OB1 association, suggesting dynamical influence by the Ori OB1 association. If such a cometary structure is formed by photoevaporation from nearby OB stars, we may also find a velocity gradient in the sense that the "head" is moving more slowly than the tail with respect to the ionizing stars (Bertoldi 1989; Bertoldi, McKee 1990). In order to see whether such a velocity gradient is present, we checked the velocity structure of the cloud (figure 7a). As a result, we found a small velocity gradient of ~ 0.3 km s^{-1} pc^{-1} in ^{13}CO, which may be the result of an interaction. To summarize, the shape and the geometry of the cloud suggest that the cloud is likely to be physically associated with Ori OB1.

Table 4. Physical properties of the ^{13}CO cores.

Cloud name	Distance (pc)	z (pc)	T_{ex} (K)	τ_{13}*	N_{13}*†	$\langle N(H_2)\rangle$†	$n(H_2)$†	Mass ($M_\odot$)	R (pc)	ΔV_{comp} (km s^{-1})	M_{vir} ($M_\odot$)	L ($L_\odot$)
G 208.3−28.4	460	230	16	0.47	5.3	1.7	0.8	31	0.50	0.82	71	6
G 203.5−24.7	460	200	21	0.62	27.0	9.1	4.6	146	0.48	1.93	372	187
G 206.4−25.9	460	210	16	0.66	9.7	3.5	1.3	100	0.64	1.01	137	9
G 239.2−16.3	1500	430	9	0.67	2.5	0.9	0.2	75	1.10	0.96	212	46
G 316.4+21.2	630	230	20	0.52	17.5	7.1	3.0	172	0.59	1.51	279	91

*The optical depth and column density are for the peak position of each ^{13}CO core.
†Units for N_{13}, $\langle N(H_2)\rangle$, and $n(H_2)$ are 10^{15} cm^{-2}, 10^{21} cm^{-2}, and 10^3 cm^{-3}, respectively.

Table 5. Physical properties of the C^{18}O cores.

Cloud name	Distance (pc)	z (pc)	T_{ex} (K)	τ_{18}*	N_{18}*†	$\langle N(H_2)\rangle$†	$n(H_2)$†	Mass ($M_\odot$)	R (pc)	ΔV_{comp} (km s^{-1})	M_{vir} ($M_\odot$)	L ($L_\odot$)
G 208.3−28.4-East.....	460	230	16	0.12	4.6	3.3	2.0	37	0.40	0.48	19	...
G 208.3−28.4-Center....	460	230	16	0.11	4.9	3.6	3.3	17	0.26	0.51	14	6
G 203.5−24.7.....	460	200	21	0.10	38.1	16.7	11.0	161	0.37	1.25	121	187
G 206.4−25.9.....	460	210	16	0.16	14.1	7.5	3.8	120	0.48	0.65	42	9
G 239.2−16.3.....	1500	430	9	0.10	2.1	2.5	1.3	43	0.49	0.49	25	46
G 316.4+21.2.....	630	230	20	0.10	29.4	14.9	7.1	268	0.51	1.46	226	91

*The optical depth and column density are for the peak position of each C^{18}O core.
†Units for N_{18}, $\langle N(H_2)\rangle$, and $n(H_2)$ are 10^{14} cm^{-2}, 10^{21} cm^{-2}, and 10^3 cm^{-3}, respectively.

3.3.2. 05044−0325 (G 203.5−24.7)

This IRAS source is also located west to the Orion molecular clouds. The source is located within the dark cloud L 1615/1616, and is associated with a reflection nebula, NGC 1788(= DG 51, vdB 33, RNO 35, LBN 916), illuminated by a star cluster. The source is also listed in the catalogue of remnant clouds in the Ori OB1 association (no. 3; Ogura, Sugitani 1998) and we thus assumed the distance to be 460 pc. Observations in ^{12}CO and ^{13}CO toward the reflection nebula were made by Knapp et al. (1977). The molecular cloud associated with this source was also observed in a CO survey in Orion and Monoceros (no. 13; Maddalena et al. 1986). Mapping observations in ^{12}CO and ^{13}CO were made by Ramesh (1995). He found that the cloud has a cometary shape with a dense "head" pointing toward the Ori OB1 association, and that the reflection nebula is located at the edge of the molecular cloud facing the association.

Our observations confirmed the cometary shape and the geometry of the cloud. However, we found no clear velocity gradient along the major axis although the tail seems to have a little more positive velocity than the head (figure 7b). The absence of a velocity gradient can be understood if the cloud is moving perpendicular to the line of sight, but we only suggest that the cloud may be physically associated to the Ori OB1 association.

3.3.3. 05050−0614 (G 206.4−25.9)

This source is located at the head of the Cometary Complex-A, $\sim 3°$ north of G 208.3−28.4 described in subsection 3.3.1. A reflection nebula RNO 37(= DG 52) is associated with the source. This molecular cloud was observed in ^{13}CO by Bally et al. (1991); they found that the cloud has a cometary shape with a dense "head" pointing toward the Ori OB1 association. Our observations confirmed the cometary shape of the cloud, and showed that the peak intensity position of the cloud is 2′ west of the IRAS position, i.e., the IRAS source is located at the edge of the molecular cloud facing the Ori OB1 association, a situation similar to G 203.5−24.7. We also found a small velocity gradient of ~ 0.13 km s^{-1} pc^{-1} in ^{13}CO (figure 7c). We suggest from the shape and the geometry that the cloud is likely influenced by the Ori OB1 association.

3.3.4. 06345−3023 (G 239.2−16.3)

The optical appearance of the source consists of more than 2 stars surrounded by diffuse nebulosity. The nebulosity is listed in Gyulbudaghian, Rodríguez, and Villanueva (1993). The structure in the IRAS 100 μm image put the source in the catalog of comet-like IRAS sources (G 239−15; Odenwald, Rickard 1987). However, little is known about the source. About 3° north-east of the source, reflection nebulae vdB 83 and vdB 84 exist, but it is not clear whether these objects are related to

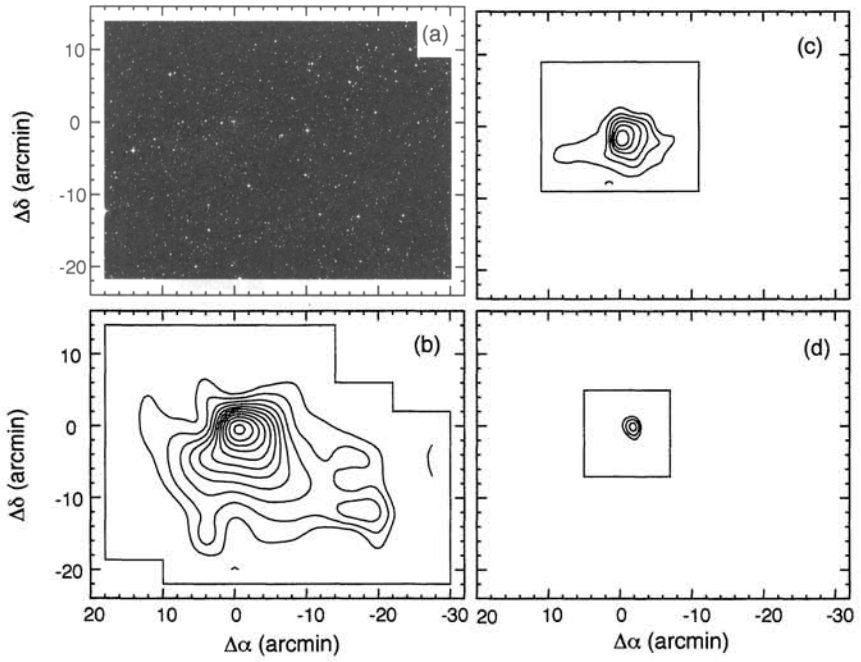

Fig. 5. Same as figure 2, but for IRAS 06345−3023 (G 239.2−16.3). The contour levels are every 0.85 K km s^{-1} (3σ), starting from 0.85 K km s^{-1} (3σ) in ^{12}CO, every 0.36 K km s^{-1} (3σ), starting from 0.36 K km s^{-1} (3σ) in ^{13}CO, and every 0.045 K km s^{-1} (1σ), starting from 0.135 K km s^{-1} (3σ) in C^{18}O.

the IRAS source, and again little is known about these nebulae.

At a larger scale, a Wolf–Rayet star WR 6 exists about 7° north-east of the source. WR 6 is thought to be the exciting star of the H II regions S 303, S 304, and S 308 (Chu 1981; Chu et al. 1982). An open cluster Collinder 121 exists at the same line of sight, but it is still unclear whether WR 6 is a member of the cluster. WR 6 and/or Collinder 121 are candidate objects which are physically associated with the IRAS source. The distance of WR 6 is controversial; probably in the range 600–3000 pc (see e.g., Arnal, Cappa 1996; de Zeeuw et al. 1999).

Our observations have revealed dense gas around the IRAS source, suggesting that the cloud is a site of recent star formation. We estimated the distance from a galactic rotation curve (Wouterloot et al. 1990) and adopted the kinematic distance of 1.5 kpc as the cloud distance. At the distance, the source is away from the galactic plane by $\sim$ 430 pc, which is about 5-times larger than the half thickness at half maximum of the CO gas (Dame et al. 1987). The origin of the isolated star-forming cloud at such a large distance from the galactic plane deserves future study.

3.3.5. 13543−3941 (G 316.4+21.2)

This source is located in the cometary globule CG 12. The head is at the north-west and the tail is at the south-east. A reflection nebula NGC 5367 is located at the head of the cloud. The origin of the cometary shape is not known. A supernova explosion near (l, b) = (320°, 30°) about 10^7 yr ago may have formed the present shape (Williams et al. 1977). The distance of the cloud was estimated to be 630 pc (Williams et al. 1977). Observations in ^{12}CO and ^{13}CO were made by van Till, Loren, and Davis (1975). High-resolution CO and C^{18}O (J = 2–1) observations were made and a molecular outflow was found (White 1993). We found that the cloud has a cometary shape with the head at NW and the peak intensity position of the cloud is located at $\sim$ 2′ E from the IRAS source, i.e., the IRAS source is located at the edge of the molecular cloud opposite to the tail, though no clear velocity gradient is seen in the present map (figure 7d).

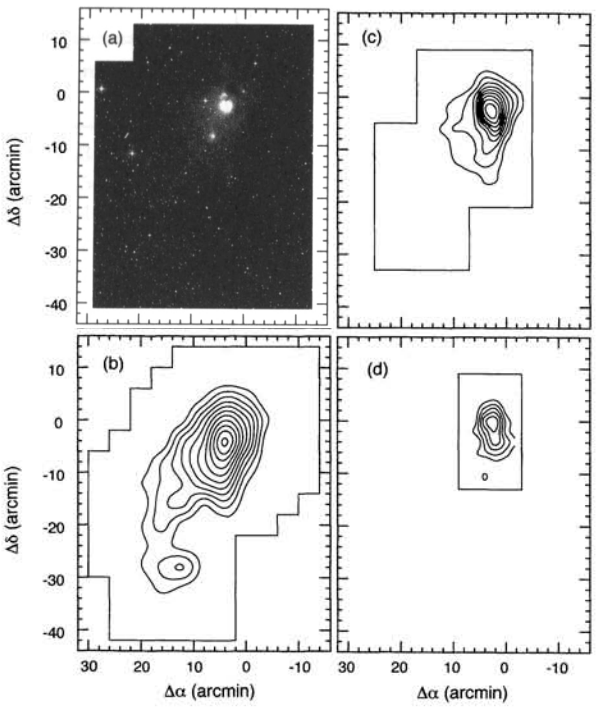

Fig. 6. Same as figure 2, but for IRAS 13543−3941 (G 316.4+21.2). The contour levels are every 3.17 K km s^{-1} (10σ), starting from 3.17 K km s^{-1} (10σ) in ^{12}CO, every 1.3 K km s^{-1} (10σ), starting from 1.3 K km s^{-1} (10σ) in ^{13}CO, and every 0.4 K km s^{-1} (5σ), starting from 0.4 K km s^{-1} (5σ) in C^{18}O.

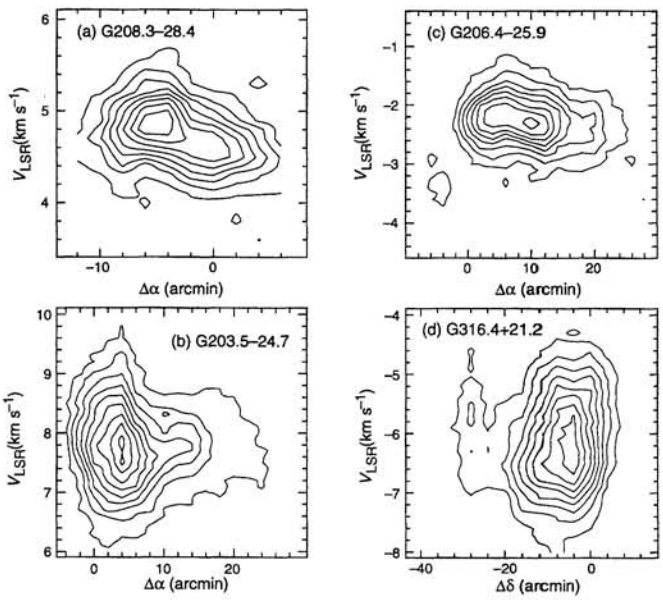

Fig. 7. (a) A position–velocity map of G 208.3−28.4 in ^{13}CO. The map was made by integrating all observed points along the minor axis (declination). The contours are every 0.05 K deg, starting from 0.05 K deg. (b) Same as (a) but for G 203.5−24.7. The contours are every 0.1 K deg, starting from 0.1 K deg. (c) Same as (a) but for G 206.4−25.9. The contours are every 0.1 K deg, starting from 0.1 K deg. (d) Same as (a) but for G 316.4+21.2 in ^{12}CO. Integration was made along the minor axis (right ascension). The contours are every 0.3 K deg, starting from 0.3 K deg.

4. Discussion

4.1. Characteristics of the Detections and Nondetections

In this subsection, we first discuss the characteristics of the detections and nondetections. By inspecting optical images, we found sources associated with nebulosities, which are likely to be reflection nebulae, tend to have associated molecular clouds; 5 of 6 IRAS sources with nebulosities have associated molecular clouds. We also compared the infrared colors of the detections and nondetections in figure 8. No significant differences were found in the infrared colors. The results indicate that the association of the optical nebulosities to IRAS sources can be used to choose young stellar objects effectively among IRAS sources.

Here we consider the nature of nondetections. Since the detection limit is $\sim 0.02\,M_\odot$ at a distance of 100 pc, we examined whether a molecular cloud with $M \lesssim 0.02\,M_\odot$ could be a parent molecular cloud of an IRAS source with $L \sim 0.1\,L_\odot$, a typical value of the present target. A computation of pre–main-sequence evolutionary tracks (D'antona, Mazzitelli 1994) showed that even at the earliest stage of evolution ($\sim 10^4$ yr), a star with $M \lesssim 0.02\,M_\odot$ cannot have a luminosity of $\sim 0.1\,L_\odot$. Moreover, if the source comprises a star with $M = 0.02\,M_\odot$, the star-formation efficiency reaches $\sim 50\%$, extremely higher compared to the typical value of a few percent. Although it is possible that parent molecular gas has been dissipated after star formation, dissipating most of the material in such a short time must be quite difficult for such a low-mass star. Thus, it is most likely that nondetections do not represent young stellar objects, but indicate extragalactic sources or planetary nebulae. Indeed, the infrared colors of the nondetections are similar to those of planetary nebulae (figure 9). Further observations, such as deep imaging, spectroscopy, and H I observations, are needed to reveal the nature of the nondetections and to better establish selection criteria for young stellar objects.

The fact that 4 of the 5 detections have a cometary shape should be given attention. These clouds may have

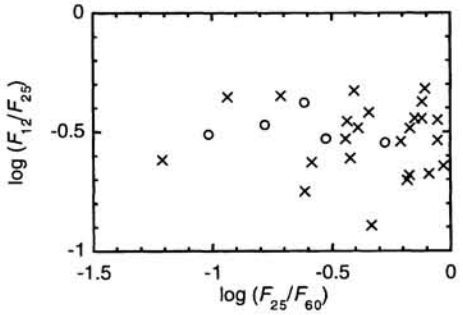

Fig. 8. Two-color diagram for 29 IRAS point sources. The open circles and crosses represent CO detections and nondetections, respectively.

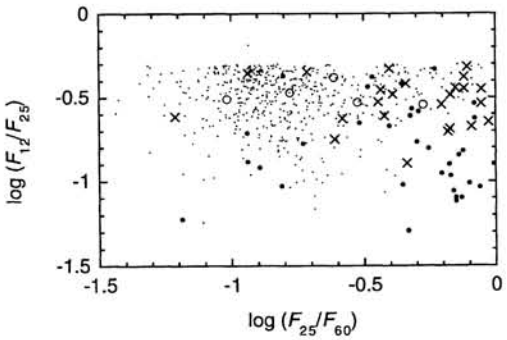

Fig. 9. Two-color diagram for the detections (open circles), nondetections (crosses), sources identified as extragalactic objects (small dots), and planetary nebulae (filled circles). The colors of the nondetections are similar to those of planetary nebulae.

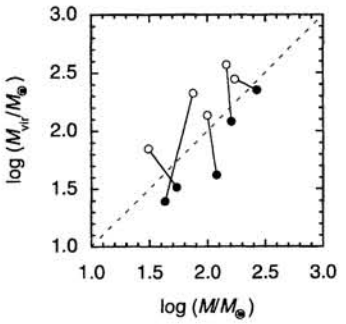

Fig. 10. Virial mass ($M_{\rm vir}$) plotted against the LTE mass (M) of the ^{13}CO cores (open circles) and C^{18}O cores (filled circles). The values connected by the solid lines were calculated for the same core. The dashed line represents $M_{\rm vir} = M$. All ^{13}CO cores have $M_{\rm vir}/M > 1$, whereas all C^{18}O cores have $M_{\rm vir}/M < 1$, i.e., C^{18}O cores are gravitationally bound.

been ejected from nearby molecular clouds where OB associations were formed, or condensed from the expanding H I shells surrounding OB associations. In either case, cometary clouds can be located far away from the OB associations, i.e., active star-forming regions. Our selection criteria to exclude sources near well-known star-forming regions may preferably choose such a cometary cloud as a target, and thus the high ratio of cometary cloud in the detections might be due to the selection effect.

4.2. *Star Formation at High Latitude*

In this subsection we discuss the distribution of star-forming clouds at high latitude. We searched for molecular clouds toward IRAS point sources having infrared spectra typical of young stellar objects. At $|b| \geq 30°$, 3 sources match our selection criteria, and no molecular clouds were found. In the intermediate latitude, we found molecular clouds toward 3 out of 13 sources at $20° \leq |b| < 30°$, and 2 out of 13 at $10° \leq |b| < 20°$. Although we found a new sample of star-forming clouds unknown to date at intermediate latitude ($10° \leq |b| < 30°$), no sign of star formation is found at high latitude ($|b| \geq 30°$), which appears consistent with the previous studies. However, some possibilities of star formation in high-latitude clouds still remain; e.g., the presence of a low-mass protostar below the detection limit ($L \lesssim 0.1\,L_\odot$), which is invisible at the far-infrared wavelength. One of the ways to answer this question is to search for high-latitude clouds which are capable of star formation. Our observations show that IRAS sources with nebulosities tend to have associated molecular clouds. However, searches for molecular clouds toward optical nebulosities alone may not be sufficient, since clouds without optical counterpart are indeed found by unbiased CO surveys at high latitudes (Magnani et al. 1986; Hartmann et al. 1998). Unbiased surveys for high-latitude cloud and/or sensitive infrared observations for detected clouds may better answer the question whether high-latitude clouds are potential sites of star formation.

4.3. *Properties of Molecular Clouds*

The mass of the detected clouds estimated from the ^{13}CO observations ranges over 50–500$M_\odot$. The fraction of the ^{13}CO mass to the ^{12}CO mass ranges over 40–70% with the exception of G 239.2−16.3 (11%). The C^{18}O masses are nearly the same as those of ^{13}CO, except for G 239.2−16.3; the C^{18}O mass amounts only to $\sim 27\%$ of the ^{13}CO mass. The large fraction of dense gas to diffuse gas could be explained as a result of interactions. Diffuse gas might have disappeared as a result of interactions, whereas dense gas is effectively produced by compres-

Table 6. Average physical properties of $C^{18}O$ cores in ILCs and other star-forming regions.

Region	$\langle N(H_2)\rangle$ (10^{21} cm^{-2})	Mass ($M_\odot$)	R (pc)	ΔV_{comp} (km s^{-1})	Distance (pc)	References†
ρ Oph	17.6	90	0.24	0.87	160	1
Cha I	11.3	32	0.22	0.81	140	2
ILCs	8.1	107	0.42	0.81	460–1500	3
Tau	6.9	23	0.23	0.49*	140	4
Oph-north	5.4	14	0.19	0.72	160	1
Cha II	5.1	20	0.22	0.78	180	2
Cha III	3.6	13	0.23	0.88	180	2
L 1333	4.3	9	0.16	0.92	180	5

*Line width at the peak intensity position.
†(1) Tachihara et al. 1999; (2) Mizuno et al. 1999; (3) this work; (4) Onishi et al. 1996, 1998; (5) Obayashi et al. 1998.

sion, and thus the fraction of the dense gas has become large. The fact that only G 239.2−16.3 shows a small fraction of dense gas may be caused by beam dilution; since the source is located $\sim$ 3 times farther than the rest, $N(H_2)$ may be underestimated in the ^{13}CO and $C^{18}O$ observations and thus the ^{13}CO and $C^{18}O$ mass may be underestimated, whereas ^{12}CO does not suffer from beam dilution so much as in ^{13}CO and $C^{18}O$. The fact that the size of the cloud is $\sim$ 2 times larger than the rest of the cloud also supports this.

In the following we discuss the gravitational stability of the cores using the virial theorem. The ratio M_{vir}/M_{LTE} ranges over 1.4–2.9 in the ^{13}CO cores and 0.4–0.8 in the $C^{18}O$ cores (figure 10). All of the cores are gravitationally bound when observed in $C^{18}O$, whereas they are not gravitationally bound in ^{13}CO. This indicates that gravitationally-bound cores may exist, and thus stars can be formed within a gravitationally unbound system, such as ^{13}CO cores. The fact that ^{13}CO cores are not gravitationally bound is consistent with the results of the extensive ^{13}CO survey for molecular clouds (Fukui, Yonekura 1997; Dobashi et al. 1996; Yonekura et al. 1997; Kawamura et al. 1998). These authors find that most of ^{13}CO clouds are not gravitationally bound, even if stars are formed within the cloud. If we consider the possible existence of gravitationally-bound cores within ^{13}CO clouds, the nature of the star-forming ^{13}CO clouds with $M_{vir}/M > 1$ could be understood. Thus, it is quite important to see the physical properties of dense cores, such as $C^{18}O$ cores, in order to reveal whether star formation is occurring within the cores.

Here we compare the properties of $C^{18}O$ cores detected in the present survey (hereafter referred to as ILCs, the intermediate-latitude clouds) with $C^{18}O$ cores in Taurus (Onishi et al. 1996, 1998), Ophiuchus (Tachihara et al. 1999), Chamaeleon (Mizuno et al. 1999), and L 1333 molecular cloud (Obayashi et al. 1998) observed with the same telescope. The cores in ρ Oph, Taurus, and Chamaeleon I can be regarded as being samples of active star-forming regions, whereas those in Ophiuchus north, Chamaeleon III, and L 1333 are samples of less active regions. Table 6 gives the average properties of $C^{18}O$ cores in ILCs and other star-forming regions. The sizes of the ILCs are $\sim$ 2 times larger and the masses are $\sim$ 3 times larger than the cores in the other regions on average, whereas no clear differences are found in the line widths and the H_2 column densities. It is to be noted that the sizes of ILCs might be overestimated and that the column density might be underestimated, since the distances of ILCs are 3–10 times larger than those in the other regions. If we consider this effect, we will find that H_2 column densities of the $C^{18}O$ cores in the active star-forming regions including ILCs are larger than those in less active region, whereas no clear differences will be find in ΔV, M, and R. This result is consistent with the previous studies, and thus a high column density is the general trend for star-forming cores.

We also investigate the ratio of the virial mass, M_{vir}, to the LTE mass, M_{LTE}. For all $C^{18}O$ cores in ILCs, M_{vir}/M_{LTE} is smaller than 1. This is consistent with previous studies. In L 1333, the cloud associated with the youngest IRAS source has the smallest M_{vir}/M_{LTE} ratio of $\sim$ 1. They suggested that star formation may occur preferentially in a cloud whose internal kinetic energy is the smallest compared with the self-gravitational energy. In Ophiuchus, all star-forming $C^{18}O$ cores are distributed in a range of $M_{vir}/M < 1$. In Chamaeleon, star-forming cores are almost in virial equilibrium. Considering that ILCs are sites of star formation, the present results support that star formation tends to occur in a cloud with a small M_{vir}/M_{LTE} ratio.

In summary, we can conclude that star-forming clouds tend to have a high column density, as well as a smaller M_{vir}/M_{LTE} ratio.

5. Conclusion

In order to find a sample star-forming cloud unknown to date at intermediate-to-high galactic latitude, we made a search for molecular clouds toward 29 IRAS sources in ^{12}CO ($J = 1$–0). Targets were selected mainly from the infrared properties of the sources. The main results can be summarized as follows:

(1) Five sources among 29 have associated molecular cloud, i.e., 04591−0856, 05044−0325, 05050−0614, 06345−3023, and 13543−3941. Among 5 detections, the molecular cloud associated with 06345−3023 (G 239.2−16.3) was detected for the first time. If we assume a distance of 1.5 kpc, this source is $\sim$ 430 pc away from the galactic plane. Three sources 04591−0856 (G 208.3−28.4), 05044−0325 (G 203.5−24.7), and 05050−0614 (G 206.4−25.9)) are located west to the Orion molecular clouds, and 13543−3941 (G 316.4+21.2) is located in the cometary globule CG 12. Four of the 5 detections show a cometary shape with a "head-tail" distribution, and three of them have the IRAS source located at the edge opposite to the tail.

(2) We found that all of the detections are associated with optical nebulosities, which are likely to be reflection nebulae.

(3) We compared the properties of the clouds detected in the present survey to those in Ophiuchus, Taurus, Chamaeleon, and L 1333. We found that star-forming clouds tend to have a high column density, as well as a smaller $M_{\rm vir}/M_{\rm LTE}$ ratio.

The NANTEN project (southern 4-meter radio telescope) is based on a mutual agreement between Nagoya University and Carnegie Institution of Washington. We greatly appreciate the hospitality of all staff members of the Las Campanas Observatory of the Carnegie Institution of Washington. We also acknowledge that this project could be realized by contributions from many Japanese public donators and companies. This research has made use of the NASA/IPAC Extragalactic Database (NED) which is operated by the Jet Propulsion Laboratory, Caltech, under contract with the National Aeronautics and Space Administration. The Digitized Sky Surveys were produced at the Space Telescope Science Institute under U.S. Government grant NAGW-2166. The images of these surveys are based on photographic data obtained using the Oschin Schmidt Telescope on Palomar Mountain and the UK Schmidt Telescope. The plates were processed into the present compressed digital form with the permission of these institutions. Three of the authors (AM, HO, and YF) acknowledge financial support from the scientist exchange program under bilateral agreement between JSPS (the Japan Society for the Promotion of Science) and CONICYT (the Chilean National Commission for Scientific and Technical Research). This work was financially supported in part by Grants-in-Aid for Scientific Research from JSPS (Nos. 10044076, 11740125).

References

Arnal E.M., Cappa C.E. 1996, MNRAS 279, 788
Bally J., Langer W.D., Wilson R.W., Stark A.A., Pound M.W. 1991, in Fragmentation of Molecular Clouds and Star Formation, ed E. Falgarone, F. Boulanger, G. Duvert (Kluwer, Dordrecht) p11
Bertoldi F. 1989, ApJ 346, 735
Bertoldi F., McKee C.F. 1990, ApJ 354, 529
Blitz L., Magnani L., Mundy L. 1984, ApJ 282, L9
Chu Y.H. 1981, ApJ 249, 195
Chu Y.H., Gull T.R., Treffers R.R., Kwitter K.B., Troland T.H. 1982, ApJ 254, 562
Combes F. 1991, ARA&A 29, 195
Dame T.M., Ungerechts H., Cohen R.S., de Geus E.J., Grenier I.A., May J., Murphy D.C., Nyman L.-Å., Thaddeus P. 1987, ApJ 322, 706
D'antona F., Mazzitelli I. 1994, ApJS 90, 467
de Zeeuw P.T., Hoogerwerf R., de Bruijne J.H.H. 1999, AJ 117, 354
Dickman R.L. 1978, ApJS 37, 407
Dobashi K., Bernard J.-P., Fukui Y. 1996, ApJ 466, 282
Dobashi K., Bernard J.-P., Yonekura Y., Fukui Y. 1994, ApJS 95, 419
Emerson J.P. 1987, in Star Forming Region, ed M. Peimbert, J. Jugaku (Kluwer, Dordrecht) p19
Frerking M.A., Langer W.D., Wilson R.W. 1982, ApJ 262, 590
Fukui Y., Yonekura Y. 1997, in New Horizons from Multi-Wavelength Sky Surveys, ed B.J. McLean, D.A. Golombek, J.J.E. Hayes, H.E. Payne (Kluwer, Dordrecht) p165
Gyulbudaghian A.L., Rodríguez L.F., Villanueva V.M. 1993, Rev. Mex. Astron. Astrofis. 25, 19
Hartmann D., Magnani L., Thaddeus P. 1998, ApJ 492, 205
Heyer M.H., Brunt C., Snell R.L., Howe J.E., Schloerb F.P. Carpenter J.M. 1998, ApJS 115, 241
Kawamura A., Onishi T., Yonekura Y., Dobashi K., Mizuno A., Ogawa H., Fukui Y. 1998, ApJS 117, 387
Keto E.R., Myers P.C. 1986, ApJ 304, 466
Knapp G.R., Kuiper T.B.H., Knapp S.L., Brown R.L. 1977, ApJ 214, 78
Maddalena R.J., Morris M., Moscowitz J., Thaddeus P. 1986, ApJ 303, 375
Magnani L., Blitz L., Mundy L. 1985, ApJ 295, 402
Magnani L., Caillault J.-P., Buchalter A., Beichman C.A. 1995, ApJS 96, 159
Magnani L., Hartmann D., Speck B.G. 1996, ApJS 106, 447
Magnani L., Lada E.A., Blitz L. 1986, ApJ 301, 395
Magnani L., Onello J.S. 1995, ApJ 443, 169
Mizuno A., Hayakawa T., Tachihara K., Onishi T., Yonekura Y., Yamaguchi N., Kato S., Hara A. et al. 1999, PASJ 51, 859

Myers P.C., Fuller G.A., Mathieu R.D., Beichman C.A., Benson P.J., Schild R.E., Emerson J.P. 1987, ApJ 319, 340
Obayashi A., Kun M., Sato F., Yonekura Y., Fukui Y. 1998, AJ 115, 274
Odenwald S.F., Rickard L.J. 1987, ApJ 318, 702
Ogawa H., Mizuno A., Hoko H., Ishikawa H., Fukui Y. 1990, Int. J. Infrared Millimeter Waves 11, 717
Ogura K., Sugitani K. 1998, Publ. Astron. Soc. Aust. 15, 91
Onishi T., Mizuno A., Kawamura A., Ogawa H., Fukui Y. 1996, ApJ 465, 815
Onishi T., Mizuno A., Kawamura A., Ogawa H., Fukui Y. 1998, ApJ 502, 296
Pottasch S.R. 1992, A&AR 4, 215
Ramesh B. 1995, MNRAS 276, 923
Stacy J.G., Myers P.C., de Vries H.W. 1989, in the Physics and Chemistry of Interstellar Molecular Clouds, ed G.Winnewisser, J.T. Armstrong (Springer-Verlag, Berlin) p117
Tachihara K., Mizuno A., Fukui Y. 1999, ApJ in press
van Till H., Loren R., Davis J. 1975, ApJ 198, 235
White G.J. 1993, A&A 274, L33
Williams P.M., Brand P.W.J.L., Longmore A.J., Hawarden T.G. 1977, MNRAS 180, 709
Wouterloot J.G.A., Brand J., Burton W.B., Kwee K.K. 1990, A&A 230, 21
Yonekura Y., Dobashi K., Mizuno A., Ogawa H., Fukui Y. 1997, ApJS 110, 21